TISSUE ENGINEERING: Part C
Volume 19, Number 7, 2013

DOI: 10.1089/ten.tec.2012.0472

Biomimetic Three-Dimensional Anisotropic Geometries by Uniaxial Stretch of Poly(ε-Caprolactone) Films for Mesenchymal Stem Cell Proliferation, Alignment, and Myogenic Differentiation

Zu-yong Wang, MS,[1,*] Erin Yiling Teo, PhD,[1,*] Mark Seow Khoon Chong, PhD,[2] Qin-yuan Zhang, BE,[1] Jing Lim, ME,[3] Zhi-yong Zhang, PhD,[1] Ming-hui Hong, PhD,[4] Eng-san Thian, PhD,[1] Jerry Kok Yen Chan, PhD,[2,5,6] and Swee-Hin Teoh, PhD[1,3]

Anisotropic geometries are critical for eliciting cell alignment to dictate tissue microarchitectures and biological functions. Current fabrication techniques are complex and utilize toxic solvents, hampering their applications for translational research. Here, we present a novel simple, solvent-free, and reproducible method via uniaxial stretching for incorporating anisotropic topographies on bioresorbable films with ambitions to realize stem cell alignment control. Uniaxial stretching of poly(ε-caprolactone) (PCL) films resulted in a three-dimensional micro-ridge/groove topography (inter-ridge-distance: ~6 μm; ridge-length: ~90 μm; ridge-depth: 200–900 nm) with uniform distribution and controllable orientation by the direction of stretch on the whole film surface. When stretch temperature (T_s) and draw ratio (*DR*) were increased, the inter-ridge-distance was reduced and ridge-length increased. Through modification of hydrolysis, increased surface hydrophilicity was achieved, while maintaining the morphology of PCL ridge/grooves. Upon seeding human mesenchymal stem cells (hMSCs) on uniaxial-stretched PCL (UX-PCL) films, aligned hMSC organization was obtained. Compared to unstretched films, hMSCs on UX-PCL had larger increase in cellular alignment (>85%) and elongation, without indication of cytotoxicity or reduction in cellular proliferation. This aligned hMSC organization was homogenous and stably maintained with controlled orientation along the ridges on the whole UX-PCL surface for over 2 weeks. Moreover, the hMSCs on UX-PCL had a higher level of myogenic genes' expression than that on the unstretched films. We conclude that uniaxial stretching has potential in patterning film topography with anisotropic structures. The UX-PCL in conjunction with hMSCs could be used as "basic units" to create tissue constructs with microscale control of cellular alignment and elongation for tissue engineering applications.

Introduction

Proper tissue function and regeneration rely on robust spatiotemporal control of cellular microenvironments.[1] *In vivo*, many tissues, such as skeletal and myocardial muscles, blood vessels, nerves, as well as bone, are physiologically anisotropic, with architectures consisting of highly aligned cells and cell matrices.[2,3] Such alignment plays an important role in dictating tissue functions. For example, the aligned organization of cardiomyocytes and fibroblasts is critical to the electrical and mechanical properties of the heart,[4] whereas circumferential alignment of smooth muscle cells (SMCs) in blood vessels is required for the generation of contractile force and modulation of vascular tone.[5,6] However, the inability of scaffolds to guide cell behaviors has often resulted in poor cell and cell-matrix organization.[7,8] Tissue constructs based on such scaffolds had limited ability to recreate anisotropic tissues with aligned cells and cell matrices.

Scaffolds with versatile topographical geometries have been shown to deliver cell-matrix-regulator signals to regulate

[1]Department of Mechanical Engineering, National University of Singapore, Singapore, Singapore.
[2]Department of Obstetrics and Gynaecology, Yong Loo Lin School of Medicine, National University of Singapore, Singapore, Singapore.
[3]Division of Bioengineering, School of Chemical and Biomedical Engineering, Nanyang Technological University, Singapore, Singapore.
[4]Department of Electrical and Computer Engineering, National University of Singapore, Singapore, Singapore.
[5]Department of Reproductive Medicine, KK Women's and Children's Hospital, Singapore, Singapore.
[6]Cancer and Stem Cell Biology, Duke-NUS Graduate Medical School, Singapore, Singapore.
*The first two authors contributed equally to this work.

cell behaviors, and serve as powerful artificial microenvironments for recapitulating tissue architectures and functions.[1,9] Anisotropic topography, typically consisting of highly orientated fibrils and ridge/grooves, provides an effective approach to mimic the cellular microenvironments *in vivo* for eliciting cell alignment.[10,11] Through interaction with the anisotropic topography, cells have been found to rearrange cytoskeletons, alter their morphologies, and self-organize into aligned structures via a mechanism known as contact guidance.[10–13] This alignment has been observed in different cell types, including epithelial cells,[14] SMCs,[15] nerve cells,[11] and various stem cells.[16–18] In particular, the anisotropic topography could impact upon functional performance parameters such as cell adhesion/proliferation,[14] elongation,[19] mobility,[20] differentiation,[10,16,21] and hierarchical engineered tissue mechanics.[13]

Poly(ε-caprolactone) (PCL) is a most used synthetic polymer in biomedicine, with desirable properties of biocompatibility, bioresorbability, and low cost.[22] Moreover, PCL films are flexible, with unique capability to allow incorporation of desired physicochemical characteristics,[23] and hence find widespread applications in tissue engineering (TE).[24–26] It is now becoming more apparent that precise control of seeded cells is crucial for successful applications of PCL films in regenerating functional tissues that require aligned cell and cell-matrix organization.[24–26] Many groups have leveraged on the effects of incorporating anisotropic topographies on PCL films.[11,27,28] The two main strategies include soft-lithography and electrospinning. Although they are feasible for preparation, anisotropic topographies generated from soft-lithography typically require mechanical separation of PCL films from the mold, which often results in formation of defects on the surface features.[29] In addition, this technique refers to a complementary set of patterning tools and processes.[30,31] Modified electrospinning setups using a rotating mandrel or void gap have been used to generate orientated PCL nanofibrous meshes. However, the poor mechanical properties of such films remain a concern. In particular, both soft-lithography and electrospinning methods use chemical solvents (e.g., chloroform, tetrahydrofuran, acetone, and ethyl acetate),[11,27,29] and the potential risk of residuals leads to problems with regard to safety considerations. Hence, it is imperative to develop an alternative strategy that eliminates the use of solvents for preparing PCL films with anisotropic topographies in a reproducible and simple way.

In this study, we present a novel method using uniaxial stretching to create orientated three-dimensional (3D) microridge/groove topographies on PCL thin films. This technique allows fabrication of anisotropic topography in a solvent-free, reproducible, and simple way. The induced anisotropic topography will be demonstrated to have robust capability for aligning and elongating human mesenchymal stem cells (hMSCs) in a controllable direction.

Materials and Methods

Preparation of PCL films

PCL (MW 80,000) pellets were passed through a two-roll mill to obtain solid mass. Heat-pressed PCL films (HP-PCL, ~120 μm in thickness) were obtained though heat press of the solid mass at 80°C, 300 MPa.[32] Uniaxial-stretched PCL (UX-PCL; ~30 μm in thickness) was prepared using a proprietary solvent-free method (US Provisional Patent, No.: 61/541,201), as described in Figure 1A. Briefly, HP-PCL was cut into rectangular pieces ($5\times3\,cm^2$), heated to 54°C, and subjected to uniaxial stretching, followed by cooling down to 21°C. To investigate the influences of stretching temperature (T_s) and draw ratio (*DR*), uniaxial stretching was carried out at different T_s with constant *DR* or different *DR* with constant T_s. Otherwise, all UX-PCL was generated at constant T_s of 54°C and *DR* of 4. Since PCL is hydrophobic, alkaline hydrolysis was employed as previously described to obtain desired hydrophilicity for cell attachment.[22,33] Briefly, both HP- and UX-PCL were treated with NaOH solution (3 M) for different time of 0, 3, 12, and 48 h. All materials used were purchased from Sigma-Aldrich unless otherwise stated.

Topographical characterizations

Morphology of PCL films was characterized by light microscopy (Olympus; MX50T-F). Detailed information was obtained by field emission scanning electron microscopy (FESEM, S-4300; Hitachi) and atomic force microscopy (AFM, MFP-3D; Asylum Research).

FESEM characterization. PCL film samples were sputter-coated with gold at 10 mA for 30 s. Images were taken for surface information at a high voltage of 15 kV with different magnifications. For the analysis of morphology consistency, representative areas ($2\times2\,mm^2$) of UX-PCL were selected along two directions: (1) from the film center to the edge, and (2) from the film center to the two ends with distance between two regions of ~2 cm (Fig. 1B). Ridge orientation, inter-ridge-distance, and ridge-length were measured using the built-in functions of NIH ImageJ. Briefly, angle variation was described as the mean of standard variations of ridge orientation on different UX-PCL samples. The ridge-length was determined by drawing a straight line from the start point to the end point of individual ridge. The inter-ridge-distance was measured by drawing a line perpendicular to the ridges, and was equal to the length of the line divided by the crossed-ridge number. Four samples were used for each of the measurements above.

AFM characterization. Before characterization, samples were washed with deionized water and dried in a dry cabinet overnight. Images were taken by scanning surfaces over an area of $60\times60\,\mu m^2$ using a tapping mode and analyzed by Igor Pro6. Topographical profiles were obtained along lines perpendicular to the ridges.

Polarized light microscopy and crystallinity characterizations

The effects of uniaxial stretching on the molecular chain orientation and crystallinity of PCL films were characterized by polarized light microscopy (EMM0307; Nikon) and different scanning calorimeter (DSC, DSC60; Shimadzu), respectively. DSC analysis was performed using a scanning range from 20°C to 90°C at a heating rate of 10°C/min in air ambient. The crystallinity of PCL films was determined by comparing with 100% crystalline PCL, which has an enthalpy of fusion of 139.5 J/g.[32]

Water contact angle measurements

Water contact angle (WCA) was measured using a video contact angle system (Advanced Surface Technologies; VCA2000). Images were taken 5 s after drop dispersion (drop volume = 1 μL) to allow full drop development. Measurement was carried out along two perpendicular directions on PCL films (Fig. 3A). For UX-PCL, one of the directions was parallel to ridges. Three samples and five random positions per sample were analyzed for each of the HP- and UX-PCL measurements.

Cell isolation and culture

Human tissue collection for research purposes was approved by the Domain-Specific Review Board of National Healthcare Group, in compliance with international guidelines regarding the use of fetal tissue for research.[34] In all cases, patients gave separate written consent for the use of collected tissues.

hMSCs were isolated as previously described.[34] Briefly, single-cell suspension was obtained from fetal bone marrow, flashed out of femurs using a 22-gauge needle. The suspension was then passed through cell strainer (40 μm; BD Biosciences) to remove the tissue fragment. Cells were seeded onto flask (75 mL; Nunc) with a density of 10^6 per milliliter in D10 medium. Nonadherent cells were removed with initial medium change at third day. Adherent spindle-shaped cells (hMSC) were recovered from the primary culture after 1 week. For all experiments, hMSCs used were within passage 6 (P6) at a constant seeding density of 5000 per cm^2 on PCL films (NaOH solution, 3 M, 24 h).

Cell alignment and elongation assays

Alignment and elongation of hMSCs on UX-PCL were investigated by cytoskeletal and cytoplasmic staining. HP-PCL without stretching was set as control. After 12 h, and 3, 5, 10, and 15 days of culture, cells were washed with phosphate-buffered saline (PBS). For cytoskeletal staining, hMSCs were fixed with paraformaldehyde (3.7% in PBS) for 15 min, followed by permeabilization with Triton-X 100 (0.1% in PBS) for 10 min. After blocking with bovine serum albumin solution (2% in PBS) for 30 min, cells were incubated with TRITC-conjugated phalloidin (1:200 in PBS) for 1 h to label the F-actin cytoskeleton. After washing thrice, cells were incubated with 4′-6-diamidino-2-phenylindole (1:1000) for 5 min to visualize nucleus. For cytoplasmic staining, live hMSCs were incubated with fluorescein-diacetate (FDA, 8 μg/mL) for 10 min. After removing FDA solution, cells were further incubated with propidium iodide (PI, 4 μg/mL) for 5 min, followed with PBS washing thrice. Samples after staining were immediately visualized under confocal laser scanning microscopy (CLSM, FV1000; Olympus).

Images of live cells were analyzed using the built-in function of NIH ImageJ software as previously reported.[10] For single-cell analysis, hMSCs on PCL film samples were analyzed at subconfluence. All cells in contact with other cells and cells contact with the image edges were manually removed from the data sets. Cellular arrangement angle was defined as orientation of the major elliptic axis of individual cell. Preferential cell orientation was defined as the angle that a range of 10° below and above it has the largest cell number. The preferential cell orientation was set as 0°, and all the cellular angles and ridge direction were normalized to it. Cell number within each degree from −90° to +89° was calculated, normalized such that the total sum was unity, and plotted as a curve to describe the frequency distribution of cell orientations. A perfectly isotropic sample would have a constant value 0.5556% in each degree. Cells with arrangement angles fell into ±10° were considered to be aligned.[35] A perfectly isotropic sample would be expected to have ~11.7% of the cells orientated within ±10°. Values above 11.7% indicated increased alignment. Cell elongation was described by a cell shape index (CSI, circularity = $4 \times \pi \times \text{area}/\text{perimeter}^2$), with CSI of 1 representing a circle.[10] In each measurement of control and UX-PCL groups, three samples and four random regions per sample were analyzed.

Real-time quantitative reverse transcription–polymerase chain reaction and immunocytochemistry assays

Quantitative reverse transcription–polymerase chain reaction (qRT-PCR) was performed to evaluate the interested gene expression of hMSCs. hMSCs were seeded on HP-PCL (control), UX-PCL, and tissue culture plate (TCP, 6-well; Nunc), and cultured in D10 under identical conditions for 7 and 14 days, respectively. Total RNA was extracted from cells using RNeasy mini kit (Qiagen) according to the manufacturer's instruction. The RNA concentration was determined from the optical absorbance at 260 nm (Nanodrop-N100; Thermo Scientific). cDNA was synthesized using random hexamers and Superscript III Reverse Transcriptase (Invitrogen). Real-time qRT-PCR was performed on a CFX96 real-time PCR detection system (Bio-Rad Laboratories, Inc.) for 40 cycles. Primers specific to the targeted genes (Supplementary Table S1; Supplementary Data are available online at www.liebertpub.com/tec) were obtained from primerbank (http://pga.mgh.harvard.edu/primerbank/).[17,36] Relative expression levels for the each gene targeted were determined by comparing the quantified cDNA transcript level to that of glyceraldehyde-3-phosphate dehydrogenase (used as the internal standard).[17] The results of UX-PCL and control groups were finally normalized to the relative expression levels of each gene of TCP group. Three experiments and triplicates were done. The results were analyzed using the Relative Expression Software Tool software.

Immunocytochemistry assay was performed to investigate the protein-level expression of targeted gene in hMSCs. Briefly, hMSCs were cultured on HP- (control) and UX-PCL in D10 for 7 and 14 days. Cells were fixed, penetrated, and blocked, and nucleus was visualized using the similar protocols for cytoskeleton staining (see Cell isolation and culture section). For the antibody labeling, cells after blocking were incubated with the first antibody: mouse anti-human cardiac myosin heavy chain (MHC; 1:200; Abcam), followed by incubating with second antibody Alexa Fluor® 488 goat anti-mouse immunoglobulin G (1:200; Molecular probes). Cells were analyzed by CLSM, and images were captured using identical parameters for both control and UX-PCL groups.

Cell proliferation assays

Proliferation of hMSCs on HP- and UX-PCL was investigated using colorimetric MTS assay (CellTiter 96 AQueous One solution; Promega) as previously reported.[8] TCP (24-well; Nunc) was set as control. Five samples were used for each

group. After 3, 6, and 12 days of culture, cells were washed with PBS and incubated with 20% MTS reagent in serum-free medium for 3 h at 37°C. Absorbance of the obtained dye was measured at 490 nm using a spectrophotometric plate reader (FLUOstar Optima; BMG Lab Technologies).

Statistical analyses

Data are expressed as means ± standard deviation of the mean. Statistical significance was determined for replicates of 3–5 by analysis of variance (ANOVA). One-way ANOVA with nonparametric test was used for the inter-ridge-distance and ridge-length analyses of UX-PCL, and two-way *post-hoc* Bonferroni's test was used for the other analyses. A value of $p < 0.05$ was considered statistically significant.

Results

Characterization of UX-PCL topography

Figure 1A shows the schematic of UX-PCL fabrication. The whole process, consisting of heating, uniaxial stretching, and cooling, was solvent-free. Figure 1B shows the morphologies of UX-PCL at representative regions (X-0 → X-5, Y-0 → Y-4). UX-PCL demonstrated the wave-like topographies with consistent orientations on the whole film surface. From the film center to the two ends, the topographies of representative regions showed a slight increase in the inter-ridge distance (X-0 → X-5), but no significant change was found at the regions from X-0 to X-3 ($p > 0.05$). From the film center to the edges, the topographies of representative regions showed an inconspicuous change at the regions from Y-0 to Y-3, although some reduction was observed at the region near the edge (Y-4). Highly magnified FESEM images showed that the topographies of UX-PCL were anisotropic and consisted of two distinct portions: (1) 3D microscaled ridges that were discontinuous and highly orientated along the stretching direction, with variations in ridge-angles being less than ± 1.56° (Fig. 1B, C); (2) continuous grooves that separated the ridges from each other. AFM examination revealed similar results as observed above (Fig. 1D), with height profile of ridge-depths ranging from 200 to 900 nm (Fig. 1E). In

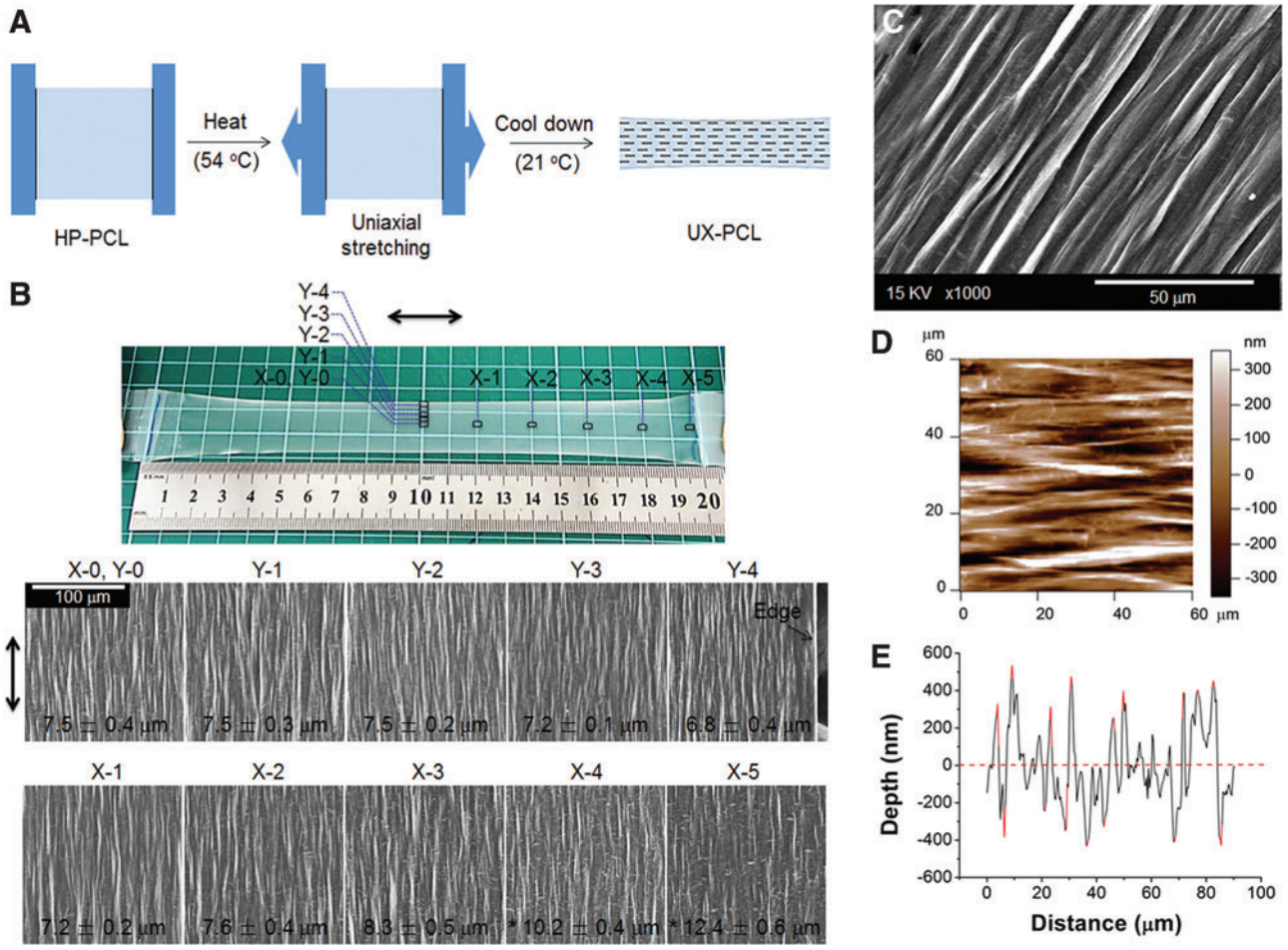

FIG. 1. Anisotropic topography of uniaxial-stretched poly(ε-caprolactone) (UX-PCL). **(A)** Schematic of fabrication. UX-PCL was generated from heat-pressed poly(ε-caprolactone) (HP-PCL) through heating (54°C), uniaxial stretching ($DR = 4$) and cooling (21°C). **(B)** Field emission scanning electron microscopy (FESEM) images of UX-PCL at representative regions (X-0 → X-5 and Y-0 → Y-4; double-headed arrow: stretching direction; Scale bar = 100 μm). UX-PCL showed anisotropic topographies on the whole film surface. *Represents the significant difference compared with the inter-ridge-distance of film central area of X-0, Y-0 ($n = 4$; $^*p < 0.05$). **(C, D)** FESEM and atomic force microscopy (AFM) images of UX-PCL (Scale bar = 50 μm). The anisotropic topographies of UX-PCL consisted of orientated micro-ridges and grooves. **(E)** Typical height profile of UX-PCL examined by AFM showed the heterogeneity of ridge-depth. Color images available online at www.liebertpub.com/tec

contrast, HP-PCL displayed relatively flat topographies (Supplementary Fig. S1A).

Influence factors on inter-ridge-distance and ridge-length

Figure 2A shows the influences of T_s and *DR* on UX-PCL topographies. With increasing T_s and *DR*, the ridge density became increasing. Quantitatively, the inter-ridge-distance exhibited similar trends in a reducing and almost linear relationship when T_s and *DR* were increased, with indication of being properly tailored in certain range (Fig. 2B). Meanwhile, the ridge-length was found to increase with increasing T_s and *DR* (Fig. 2C).

Surface hydrophilicity of UX-PCL

Figure 3A shows the measurement of WCA that was performed along two perpendicular directions. UX-PCL exhibited anisotropic surface hydrophilicity, with larger WCA along perpendicular direction than that along parallel direction (89.4° vs. 82.3°, $p < 0.001$, Fig. 3B). However, WCA of HP-PCL along the two perpendicular directions was similar (81.8° vs. 82.6°, $p > 0.05$), suggesting the presence of an isotropic surface hydrophilicity. Compared to flat PCL topography (HP-PCL), uniaxial stretching increased WCA along the perpendicular direction of UX-PCL ($p < 0.001$).

With alkaline hydrolysis, Figure 3C shows that the surface hydrophilicity of PCL films increased gradually with

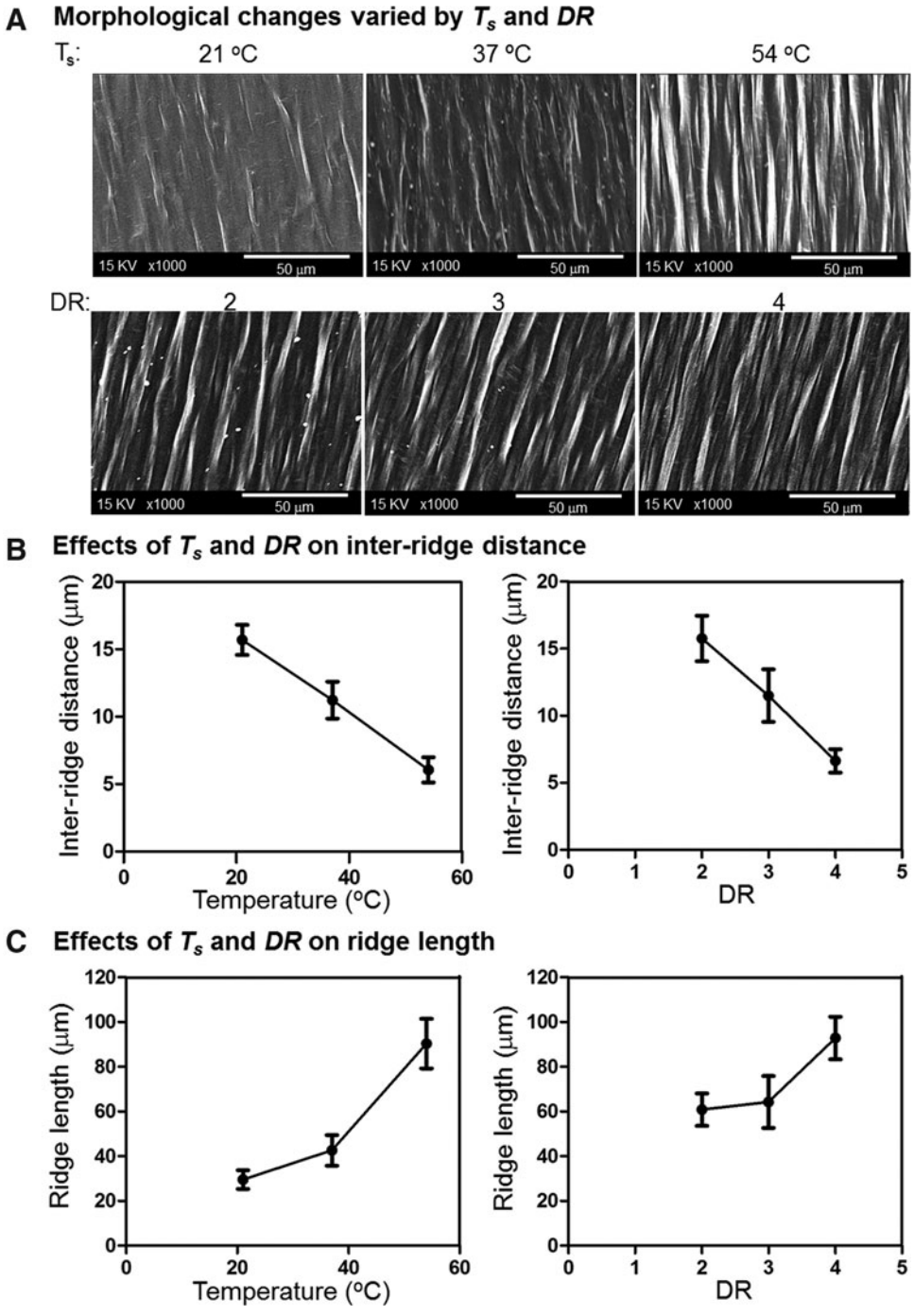

FIG. 2. Influences of T_s and *DR* on UX-PCL topography. **(A)** Morphology (scale bar = 50 μm). The morphology of UX-PCL varied with changes of T_s and *DR*. **(B)** Inter-ridge-distance. The inter-ridge-distance decreased with increasing T_s and *DR* ($n = 4$). **(C)** Ridge-length. The ridge-length increased with increasing T_s and *DR* ($n = 4$).

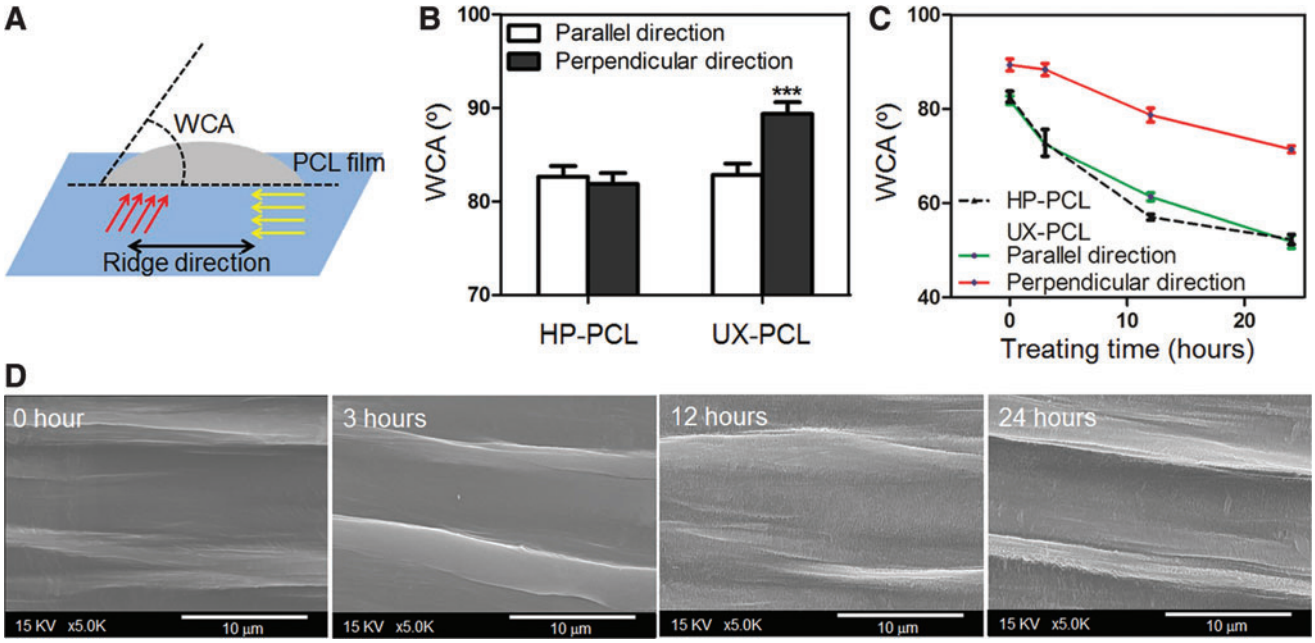

FIG. 3. Effects of surface modification on UX-PCL topography. **(A)** Schematic of water contact angle (WCA) measurement (red and yellow arrows: two perpendicular directions the WCA measurement followed; double-headed arrows: ridge direction). **(B)** WCA of HP- and UX-PCL before hydrolysis. UX-PCL revealed an anisotropic surface hydrophilicity, with a larger WCA in the perpendicular direction than that along the parallel direction. ***Represents the significant difference compared with the WCA in parallel direction ($n=3$; ***$p<0.001$). **(C)** WCA of HP- and UX-PCL after hydrolysis for different time. Alkaline hydrolysis increased the surface hydrophilicity of PCL films, and enlarged the anisotropy of surface hydrophilicity of UX-PCL with raised WCA difference between the parallel and perpendicular directions ($n=3$). **(D)** Morphology of UX-PCL after hydrolysis for different time. FESEM images showed the shapes of micro-ridge/grooves of UX-PCL being well maintained over the investigating period (scale bar = 10 μm). Color images available online at www.liebertpub.com/tec

treatment time. The WCA of UX-PCL along the parallel direction was similar as that of HP-PCL at each time point. After 24 h of treatment, the WCA within a desired range for cell growth was achieved (50°–60°).[37] The anisotropy in surface hydrophilicity of UX-PCL was seen to enlarge, with increased difference of WCA between the two perpendicular directions. At the same time, FESEM images showed higher surface roughness on UX-PCL topographies after hydrolyzed treatment, while maintaining the morphology of ridges (Fig. 3D).

hMSC alignment and elongation on UX-PCL

Performance of the anisotropic topographies on UX-PCL to modulate hMSC behavior was investigated. After 5 days of culture, hMSCs stained with F-actin (Red color) showed a highly organized alignment on UX-PCL, with orientations preferentially along the ridges (Fig. 4A). This organized alignment was found to be uniform at different regions of UX-PCL, with a directional orientation of cells observed in an area of $1\times1\,cm^2$ (Z1–Z5, Supplementary Fig. S2). In contrast, hMSCs of control (HP-PCL) did not exhibit any trend to form alignment (Fig. 4A). In parallel, to avoid potential artifacts arising from the fixation process, live staining of hMSCs using FDA/PI dyes revealed distinct alignment of cell organization on UX-PCL (green color, Fig. 4A).

Quantitatively, the angulation of hMSCs on UX-PCL was confined within a small range of −15° to +15°, with a preferential orientation approximately parallel to the ridges (Angle-shift: 1.3° ± 0.9°, Fig. 4B). In contrast, cellular arrangement angles were evenly distributed for the control group, approaching the curve of frequency distribution of a perfectly isotropic sample. Cellular elongation and alignment were then recorded as measures of hMSC organization observed above. Compared to control, hMSCs on UX-PCL exhibited significant increase in both cellular elongation (reduced CSI: 0.7× of control, $p<0.001$, Fig. 4C) and alignment efficiency (3.9× of control, $p<0.001$, Fig. 4D).

Long-term stability of aligned hMSC organization on UX-PCL

In a time-course study, hMSCs were observed to align after seeding of 12 h, with cellular arrangement angles distributed in a wide range (−30° to +10°, Fig. 5A, B). This range was observed to be narrower on day 3, with minimal changes up to day 10, indicating the self-adjustment of hMSCs in their arranged angles toward parallel to the ridges. In contrast, hMSCs in control group organized randomly over the period investigated. Quantitatively, hMSCs on both UX-PCL and control showed large CSI (>0.8) and low alignment efficiencies within the first 12 h (<35%, Fig. 5C, D). Over the period of culture, CSI of hMSCs on the anisotropic UX-PCL topographies was reduced rapidly after culture of 12 h to day 3 (1.3× reduce, $p<0.001$) and remained stable over days 3–10 (0.35 vs. 0.32, $p>0.05$, Fig. 6C). Meanwhile, the alignment efficiency was greatly increased in the period of 12 h to day 3 (1.3× increase, $p<0.001$) and exhibited slight increase in days 3–10 (80.3% vs. 85.4%, $p>0.05$, Fig. 6D). Compared to the control group, hMSCs on UX-PCL

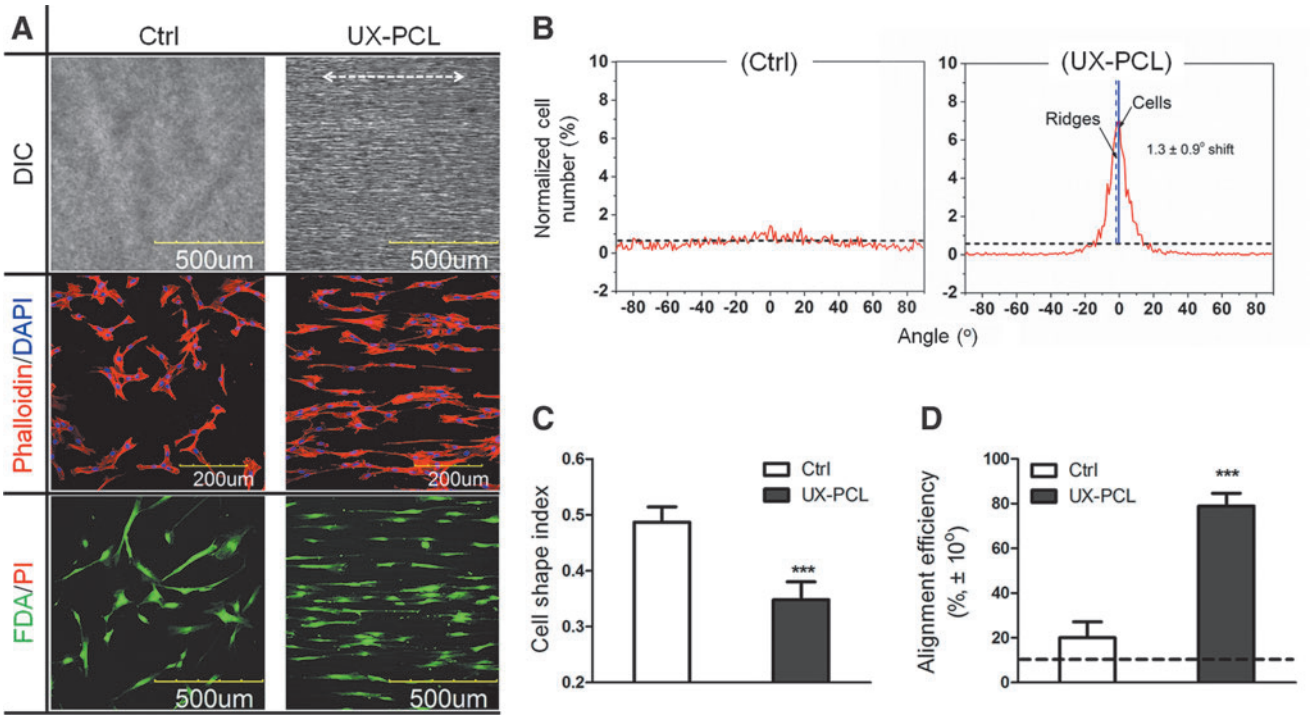

FIG. 4. Aligned organization of human mesenchymal stem cells (hMSCs) on UX-PCL. **(A)** Confocal laser scanning microscopy (CLSM) images of cytoskeletal (phalloidin: red, F-actin; 4′-6-diamidino-2-phenylindole (DAPI): blue, nucleus; scale bar = 200 μm) and cytoplasmic (fluorescein-diacetate: green, live cells; propidium iodide: red, dead cells; scale bar = 500 μm) staining of hMSCs on HP- (control) and UX-PCL (double headed white arrow: ridge direction; scale bar = 500 μm). hMSCs on UX-PCL aligned preferentially along the ridge direction, while the cells of control group organized randomly. **(B)** Frequency distribution (red lines) of hMSCs arrangement angles on control and UX-PCL (dashed blue line: ridge direction; solid blue line: preferential cell orientation). The arranged angles of hMSCs concentrated within a range of ± 15° on UX-PCL, while those of control group approximated to the angle distribution of an isotropic sample (dashed dark line). **(C, D)** Cellular elongation of hMSCs represented by cell shape index (CSI) and cellular alignment represented by the normalized cell number within ± 10° (dashed dark lines: expected values of a perfectly isotropic sample). The hMSCs on UX-PCL demonstrated lower CSI and larger alignment efficiency than the control group did. ***Represents the significant difference compared with that of control group ($n = 3$; ***$p < 0.001$). Color images available online at www.liebertpub.com/tec

showed considerable increase in the alignment efficiency (day 3, 2.8× of control, $p < 0.001$; day 10, 2.8× of control, $p < 0.001$), with a significant reduction in CSI (day 3, 0.9× of control, $p < 0.01$; day 10, 0.8× of control, $p < 0.001$). The aligned and elongated organization of hMSCs on UX-PCL was sustained for 15 days of culture, with a consistent orientation along the ridges. However, hMSCs of the control group remained randomly arranged (Supplementary Fig. S3).

Myogenic gene and protein expressions of hMSCs on UX-PCL

Efficacies of the anisotropic topographies on UX-PCL were further demonstrated by investigating their effects on the myogenic differentiation of hMSCs. Figure 6A showed the relative gene-level expressions analyzed by qRT-PCR. Compared to the control group, the hMSCs on UX-PCL demonstrated increases in the positive expressions of myogenic genes, including both early myogenic differentiation markers[17]: GATA binding protein 4 (GATA-4, 2.1× increase, $p < 0.05$) and myoblast differentiation protein 1 (MyoD-1, 1.9× increase, $p < 0.05$); late-myogenic differentiation markers[36]: cardiac β-MHC (1.1× increase, $p < 0.05$) and troponin T (Tnt, 0.9× increase, $p < 0.05$) for 7 days of culture. For 14 days of culture, the increases were observed in all the markers investigated (GATA-4: 1.9× increase, $p < 0.01$; MyoD-1: 1.8× increase, $p < 0.001$; β-MHC: 2.6× increase, $p < 0.01$; Tnt: 0.9× increase, $p < 0.01$; cardiac troponin I (TnI): 2.7× increase, $p < 0.001$).

To confirm the enhancement of myogenic differentiation observed in hMSCs on UX-PCL, immunostaining of cardiac MHC was performed. The cardiac MHC was selected because it is a mature myogenic marker and plays a critical role in the contractile machinery of cardiac muscle.[17,36] Figure 6B showed the protein-level expression of cardiac MHC in hMSCs. hMSCs demonstrated an increase in the positive expression of cardiac MHC on UX-PCL compared to that of control group for both 7 and 14 days of culture, respectively. In addition, the positive expression of cardiac MHC tended to increase with the increase of culture time of hMSCs on the anisotropic topography of UX-PCL.

Cytotoxicity and hMSC proliferation

Cytotoxicity of hMSCs on UX-PCL was evaluated by FDA/PI staining. hMSCs after 12 h, and 3, 5, 10, and 15 days of culture showed 100% FDA-stained live cells (Green color) on UX-PCL, without presence of PI-stained dead cell (red color, Figs. 4A and 5A and Supplementary Fig. S3). MTS

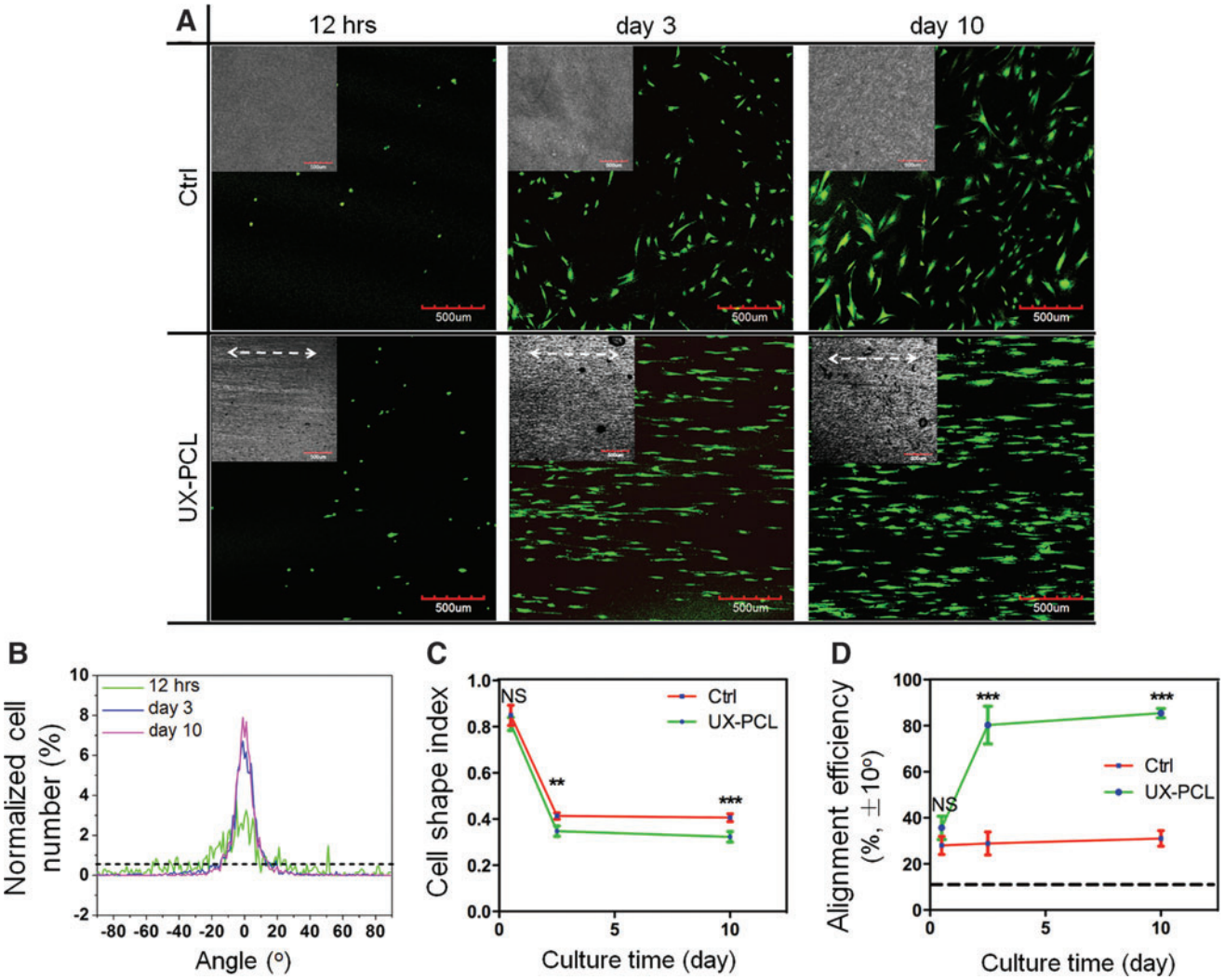

FIG. 5. Long-term effects of UX-PCL on hMSCs organization. **(A)** CLSM images of hMSCs. hMSCs aligned along the ridges on UX-PCL, but randomly organized in control group over the period investigated (Insets: HP- and UX-PCL; double-headed white arrow: ridge direction; scale bar = 500 μm). **(B)** Frequency distributions of cellular arrangement angles. The hMSCs on UX-PCL aligned into a narrower range of angles with increasing the culturing time. **(C, D)** Dynamic elongation and alignment of hMSCs. The efficiencies of elongation and alignment of hMSCs increased rapidly on UX-PCL in the initial culture period and became relatively stable for further culture. ** and ***Represent the significant difference compared with that of control group at each time point ($n = 3$; $^{**}p < 0.01$; $^{***}p < 0.001$; NS, $p > 0.05$). Dashed dark lines in **(B, D)** indicated the expected values of perfectly isotropic samples. Color images available online at www.liebertpub.com/tec

assay showed an increase in hMSC proliferation on UX-PCL over 12 days of culture, suggesting the suitability for cellular growth (day 3 vs. day 6, $p < 0.001$; day 6 vs. day 12: $p < 0.001$; Fig. 7). The proliferation of hMSCs was similar on topographies of UX-PCL and HP-PCL ($p > 0.05$), approaching that of positive control (TCP) over time (Fig. 7).

Discussion

In this study, we developed a novel technique via uniaxial stretching to create anisotropic topographical geometries on PCL thin films. The anisotropic topographies consisted of highly orientated 3D micro-ridge/grooves, with inter-ridge-distance and ridge-length being variable by T_s and DR. The anisotropic topographies enabled aligned hMSC organization on PCL films for over 2 weeks, with a significant increase in the average cell elongation, alignment, and myogenic gene expressions. Previous studies using soft-lithography and electrospinning methods have attempted to incorporate anisotropic topographies on PCL films. However, they have considerable drawbacks such as unstable yield, nonuniform geometries in a large area, tedious procedures, and/or chemical solvent usage and residualremains.[11,27,29] Our method, as described in this study, had added advantages in providing a solvent-free, reproducible, and simple fabrication for facilitating the incorporation of anisotropic topographies on PCL thin films. On the other hand, although PCL films have been used extensively in many applications previously, most of them lack functional topography geometries.[24–26] The use of uniaxial stretching has achieved unique anisotropic topographies on PCL film surfaces. This strategy could enable a whole new

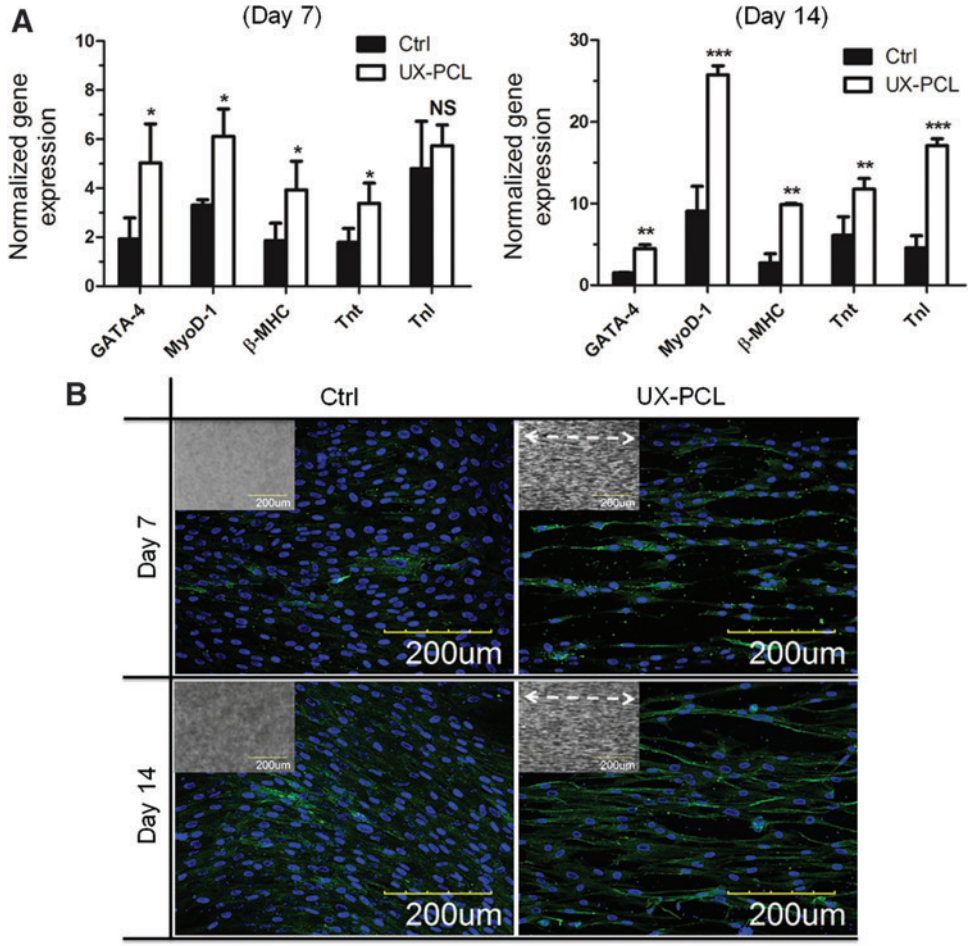

FIG. 6. Myogenic differentiation of hMSCs on UX-PCL. **(A)** Relative gene-level expression analyses of myogenic markers in hMSCs for 7 and 14 days of culture. The hMSCs on UX-PCL expressed higher level of early-myogenic differentiation markers: GATA-4 and MyoD-1, and late-myogenic differentiation markers: β-myosin heavy chain (β-MHC), Tnt and Tnl. *, ** and ***Represent the significant difference compared with the control ($n=3$; *$p<0.05$; **$p<0.01$; ***$p<0.001$; NS, $p>0.05$). **(B)** Protein-level expression analyses of late-myogenic differentiation marker: cardiac MHC in hMSCs for 7 and 14 days of culture (Insets: HP-and UX-PCL; double-headed white arrows: ridge direction; scale bar = 200 μm). The hMSCs on UX-PCL positively expressed a higher level of cardiac MHC than those of the control group, and exhibited an increased trend of expression with increasing culturing time. Color images available online at www.liebertpub.com/tec

range of complementary applications of PCL films for controlling cellular alignment and elongation in biomimetic TE.

It should be noted that uniaxial stretching in this study is applied mainly to PCL films. This method, however, could also be applicable to other thermoplastic polymers. In Supplementary Figure S4, polyethylene films after uniaxial stretching demonstrated orientated wave-like structures similarly as observed on PCL films. To the best of our knowledge, the presenting method of uniaxial stretching is suitable for semi-crystal polymers, because the formation of micro-ridges requires the polymeric crystals. In this study, uniaxial stretching resulted in the micro-ridge/grooves on PCL films. Meanwhile, it orientated the PCL molecular chains with increased film crystallinity (Fig. S1B, C), indicating a recrystallization of PCL crystals and a correlation between them and the resulted topographical structures. Slight hydrolysis of the ridge surface demonstrated parallel thorn-like structures (~50 nm of width), with orientations perpendicular to the stretching (12 h; Supplementary Fig. S1C). Such characteristics agreed with those of the multi-layered lamellas of polymeric films after uniaxial stretching.[38] Further deep degradation indicated a larger resistance of the ridges to hydrolysis, with less caves presenting on their surfaces than on the groove areas (20 days, Supplementary Fig. S1C), further suggesting that the ridges were generated from PCL crystals.[39] Because the crystalline structures are more rigid than amorphous structures, the recrystallized PCL crystals under stretching had less deformation, while the amorphous regions became thinner and formed into grooves to reveal the crystals from film surface as ridges (Schematic shown in Supplementary Fig. S1D). It should also be noted that the center of UX-PCL might experience a larger extent of stretching than the film two ends

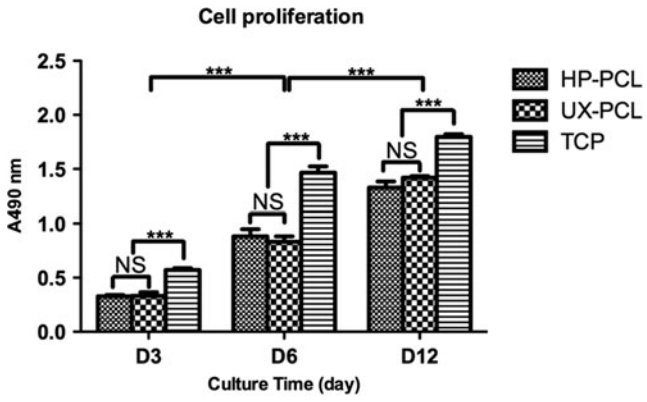

FIG. 7. Proliferation of hMSCs on HP-PCL, UX-PCL, and tissue culture plate (TCP) (positive control). The hMSCs on UX-PCL showed a similar proliferation ability as that on HP-PCL, approaching to that of TCP group with increasing the culture time ($n=5$; ***$p<0.001$; NS, $p>0.05$).

had during the initial elastic deformation. This probably resulted in the smaller inter-ridge-distance observed in film center because of larger Poisson's contraction.[40] However, most regions of UX-PCL from the center to two ends might experience similar extents of stretching, because the changes of film contraction existed mainly near film ends, and no significant difference of inter-ridge-distance was found in the regions of film central area (X-0 to X-3). Additionally, boundary effects could exist during the stretching process. In our observations, a reduction in the inter-ridge-distance was found in the regions near film edge (Y-4), probably because of the larger *DR* the edge parts experienced.[41] The reduction observed, however, was limited to film edge location and did not result in distinct morphology difference compared to the film center. In addition, all the film samples we used in this study were taken from film central area of Y-0 to Y-2 and X-0 to X-3.

The UX-PCL exhibited anisotropy in both topographical structures and surface hydrophilicity. However, due to the intrinsic properties of low melting point ($\sim$60°C) and ester bond, PCL surfaces are often delicate to undergo subsequent modification steps, such as plasma and hydrolysis treatment.[22] In our study, we show that within the period of investigation, the 3D micro-ridge/grooves UX-PCL are resistant to alkaline hydrolysis. This suggests that the anisotropic topographies conferred by uniaxial stretching could undergo proper modification for incorporating more desired physicochemical characteristics, such as RGD-peptides and CD34, on UX-PCL for particular application.[7,42] The anisotropic surface hydrophilicity observed on UX-PCL could be attributed by the increased surface roughness in perpendicular direction due to presence of the 3D micro-ridge/grooves.[43] It is worthy to note that the anisotropy of surface hydrophilicity was retained during the hydrolysis treatment. This suggests that in addition to "contact guidance," alterations to the physicochemical interactions at the biomaterial surface may be introduced to induce gradients that further influence and initiate cellular alignment.[10,44]

The biological benefits of UX-PCL were demonstrated in modulating hMSC behaviors. Here, hMSCs were selected because of their potential as a cell source for TE[45] hMSCs were able to align themselves on UX-PCL upon interaction with the anisotropic topography geometries of the film, as demonstrated by both cytoskeletal and cytoplasmic staining. Ridge-depth during the cell–substrate interaction is known to influence cellular response to a given lateral dimension.[46,47] hMSC alignment on UX-PCL suggested that the ridge-depth conferred by uniaxial stretching was able to facilitate cellular response to the anisotropic topography. A limitation of our process, as compared to other microfabrication techniques, is the inability to preciously control ridge-depth, which ranges from 200 to 900 nm in the UX-PCL. An "optimum" ridge-depth, however, remains to be elucidated, with recent studies suggesting that topography heterogeneity, rather than absolute dimensions, is more physiologically relevant.[48] Further work is warranted to better understand the influence of heterogeneous ridge-depth on hMSC response, including differentiation and function.

Cell alignment in previous studies has been relatively loosely defined, such as the cumulative cell number within ±10°,[35] ±15°,[49] and ±30°,[50] and we have employed several measures in our experiments. Although the cell–substrate interaction was influenced by topographical dimensions, our reported alignment efficiency of hMSCs (>85%, ±10°) is comparable with previous reports on PCL micropatterns,[27] and is considerably higher than those on other reported patterns (e.g., Silicon: $\sim$50%, ±10°;[35] poly (L-lactide)-PCL: <70%, ±15°[49]). It is likely that both the 3D micro-ridge/grooves and anisotropic surface hydrophilicity act as cues that contribute simultaneously to the high alignment efficiency.[10,44] Interestingly, the cell alignment as observed in our experiments was a dynamic process. hMSCs were able to adjust their orientations according to the ridges, which achieved high degrees of cellular alignment over time. It is known that substrates with microdimensions have better ability to modulate cell alignment than those with nanodimensions.[3] However, too large dimensions, particularly in groove-width larger than 50 μm, often result in delayed and low alignment efficiency, and cellular confluence is required before alignment occurs.[10,17] In comparison, hMSCs were able to align rapidly on our UX-PCL despite low density of cultured cells.

One important aspect concerning the actual applications of anisotropic topography to generate aligned tissue constructs is the consistent regulation of cues on cellular alignment. Here, we showed that the aligned hMSC organization within the entire film was remained for more than 2 weeks, with no observed reduction in the alignment efficiency, suggesting the ability of UX-PCL in facilitating long-term hMSC alignment. Moreover, the alignment orientation of hMSCs was kept consistent over time, with a controllable direction determined by the ridges. In contrast, cell alignment on chemical patterns is known to undergo changes in cellular orientations during the cell proliferation,[50] likely attributed to the preference of cells to 3D topographical structures over 2D chemical cues.[51] These thus demonstrated a consistent elicitation of UX-PCL topographies on hMSC alignment. In potential applications of engineering 3D layer-stacked cell-scaffold constructs, the orientations of cell alignment in each layer could be tailored by adjustment of placed film angles. Meanwhile, UX-PCL increased hMSC elongation as compared to its control group, with stable cellular elongation after 3 days of culture. Such consistent regulation in cellular alignment and elongation is known to have profound effects on hMSC fate, including myogenic differentiation.[17,36] In this study, the 3D anisotropic geometries on UX-PCL were found to promote hMSCs with increased expressions of myogenic genes, suggesting that UX-PCL incorporated with hMSCs may have potential for cardiac TE applications. Moreover, UX-PCL did not present any cytotoxicity but allowed hMSCs to proliferate over time. The anisotropic topographies of UX-PCL achieved robust spatial and temporal regulation of hMSC elongation, alignment, and differentiation.

Conclusions

Here, we developed a solvent-free, reproducible, and simple method via uniaxial stretching for creating anisotropic topographical geometries on bioresorbable PCL films. The incorporation of anisotropic topographies allowed for consistent control in both alignment and elongation of hMSCs, without any adverse influence on cellular proliferation. Such anisotropic topographies further promoted

hMSCs on PCL films with increased expressions of myogenic genes. Our study demonstrated that uniaxial stretching could have potential in patterning film topography for biomimetic TE applications. The PCL films of anisotropic topographies may be used as functional cues for eliciting cell alignment and elongation, as well as basic units in conjunction with stem cells for regenerating complex tissues, such as the cardiac muscle that require high cellular alignment and anisotropic functions.

Acknowledgments

The authors would like to thank following people for their generous support in this project: Yuchun Liu, Guo-Rui Jing, Tao Li, and Sandikin Dedy from National University of Singapore and Dr. Feng Wen from Nanyang Technology University, Singapore. This work was supported by grants from the Ministry of Education, Singapore (R 265-000-300-112), and the Office of Naval Research, Global (R 265-000-325-597). J.K.Y. Chan received salary support from the Singapore Ministry of Health's National Medical Research Council (CSA/012/2009).

Disclosure Statement

A filed U.S. Provisional Patent on the described technique of this article (No.: 61/541,201).

References

1. Lutolf, M.P., Gilbert, P.M., and Blau, H.M. Designing materials to direct stem-cell fate. Nature **462,** 433, 2009.
2. Beachley, V., and Wen, X. Polymer nanofibrous structures: fabrication, biofunctionalization, and cell interactions. Prog Polym Sci **35,** 868, 2010.
3. Prodanov, L., te Riet, J., Lamers, E., Domanski, M., Luttge, R., van Loon, J.J., Jansen, J.A., and Walboomers, X.F. The interaction between nanoscale surface features and mechanical loading and its effect on osteoblast-like cells behavior. Biomaterials **31,** 7758, 2010.
4. Papadaki, M., Bursac, N., Langer, R., Merok, J., Vunjak-Novakovic, G., and Freed, L.E. Tissue engineering of functional cardiac muscle: molecular, structural, and electrophysiological studies. Am J Physiol Heart C **280,** H168, 2001.
5. Krizmanich, W.J., and Lee, R.M. Correlation of vascular smooth muscle cell morphology observed by scanning electron microscopy with transmission electron microscopy. Exp Mol Pathol **64,** 157, 1997.
6. Thakar, R.G., Ho, F., Huang, N.F., Liepmann, D., and Li, S. Regulation of vascular smooth muscle cells by micropatterning. Biochem Biophys Res Commun **307,** 883, 2003.
7. Chong, M.S.K., Chan, J., Choolani, M., Lee, C.-N., and Teoh, S.-H. Development of cell-selective films for layered coculturing of vascular progenitor cells. Biomaterials **30,** 2241, 2009.
8. Jin, G., Prabhakaran, M.P., and Ramakrishna, S. Stem cell differentiation to epidermal lineages on electrospun nanofibrous substrates for skin tissue engineering. Acta Biomater **7,** 3113, 2011.
9. Kilian, K.A., Bugarija, B., Lahn, B.T., and Mrksich, M. Geometric cues for directing the differentiation of mesenchymal stem cells. PNAS **107,** 4872, 2010.
10. Aubin, H., Nichol, J.W., Hutson, C.B., Bae, H., Sieminski, A.L., Cropek, D.M., Akhyari, P., and Khademhosseini, A. Directed 3D cell alignment and elongation in microengineered hydrogels. Biomaterials **31,** 6941, 2010.
11. Xie, J., MacEwan, M.R., Li, X., Sakiyama-Elbert, S.E., and Xia, Y. Neurite outgrowth on nanofiber scaffolds with different orders, structures, and surface properties. ACS Nano **3,** 1151, 2009.
12. Curtis, A., and Wilkinson, C. Topographical control of cells. Biomaterials **18,** 1573, 1997.
13. Zorlutuna, P., Elsheikh, A., and Hasirci, V. Nanopatterning of collagen scaffolds improve the mechanical properties of tissue engineered vascular grafts. Biomacromolecules **10,** 814, 2009.
14. Karuri, N.W., Liliensiek, S., Teixeira, A.I., Abrams, G., Campbell, S., Nealey, P.F., and Murphy, C.J. Biological length scale topography enhances cell-substratum adhesion of human corneal epithelial cells. J Cell Sci **117,** 3153, 2004.
15. Cao, Y., Poon, Y.F., Feng, J., Rayatpisheh, S., Chan, V., and Chan-Park, M.B. Regulating orientation and phenotype of primary vascular smooth muscle cells by biodegradable films patterned with arrays of microchannels and discontinuous microwalls. Biomaterials **31,** 6228, 2010.
16. Lee, M.R., Kwon, K.W., Jung, H., Kim, H.N., Suh, K.Y., Kim, K., and Kim, K.-S. Direct differentiation of human embryonic stem cells into selective neurons on nanoscale ridge/groove pattern arrays. Biomaterials **31,** 4360, 2010.
17. Li, H.Q., Wen, F., Wong, Y.S., Boey, F.Y.C., Subbu, V.S., Leong, D.T., Ng, K.W., Ng, G.K.L., and Tan, L.P. Direct laser machining-induced topographic pattern promotes up-regulation of myogenic markers in human mesenchymal stem cells. Acta Biomater **8,** 531, 2012.
18. Hsu, S.H., Su, C.H., and Chiu, I.M. A novel approach to align adult neural stem cells on micropatterned conduits for peripheral nerve regeneration: a feasibility study. Artif Organs **33,** 26, 2009.
19. Teixeira, A.I., Abrams, G.A., Bertics, P.J., Murphy, C.J., and Nealey, P.F. Epithelial contact guidance on well-defined micro- and nanostructured substrates. J Cell Sci **116,** 1881, 2003.
20. Jeon, H., Hidai, H., Hwang, D.J., Healy, K.E., and Grigoropoulos, C.P. The effect of micronscale anisotropic cross patterns on fibroblast migration. Biomaterials **31,** 4286, 2010.
21. Xie, J., Willerth, S., Li, X., Macewan, M., Rader, A., Sakiyamaelbert, S., and Xia, Y. The differentiation of embryonic stem cells seeded on electrospun nanofibers into neural lineages. Biomaterials **30,** 354, 2009.
22. Woodruff, M.A., and Hutmacher, D.W. The return of a forgotten polymer-polycaprolactone in the 21st century. Prog Polym Sci **35,** 1217, 2010.
23. Xu, F.J., Wang, Z.H., and Yang, W.T. Surface functionalization of polycaprolactone films via surface-initiated atom transfer radical polymerization for covalently coupling cell-adhesive biomolecules. Biomaterials **31,** 3139, 2010.
24. Iwasaki, K., Kojima, K., Kodama, S., Paz, A.C., Chambers, M., Umezu, M., and Vacanti, C.A. Bioengineered three-layered robust and elastic artery using hemodynamically-equivalent pulsatile bioreactor. Circulation **118,** S52, 2008.
25. Giraud, M.N., Armbruster, C., Carrel, T., and Tevaearai, H.T. Current state of the art in myocardial tissue engineering. Tissue Eng **13,** 1825, 2007.
26. Chew, S.Y., Mi, R., Hoke, A., and Leong, K.W. The effect of the alignment of electrospun fibrous scaffolds on Schwann cell maturation. Biomaterials **29,** 653, 2008.
27. Sarkar, S., Lee, G.Y., Wong, J.Y., and Desai, T.A. Development and characterization of a porous micro-patterned

scaffold for vascular tissue engineering applications. Biomaterials **27,** 4775, 2006.
28. Papenburg, B.J., Vogelaar, L., Bolhuis-Versteeg, L.A.M., Lammertink, R.G.H., Stamatialis, D., and Wessling, M. One-step fabrication of porous micropatterned scaffolds to control cell behavior. Biomaterials **28,** 1998, 2007.
29. Lu, Y., and Chen, S.C. Micro and nano-fabrication of biodegradable polymers for drug delivery. Adv Drug Deliv Rev **56,** 1621, 2004.
30. Nuzzo, R.G. The future of electronics manufacturing is revealed in the fine print. PNAS **98,** 4827, 2001.
31. Shimizu, K., Fujita, H., and Nagamori, E. Alignment of skeletal muscle myoblasts and myotubes using linear micropatterned surfaces ground with abrasives. Biotechnol Bioeng **103,** 631, 2009.
32. Tiaw, K.S., Teoh, S.H., Chen, R., and Hong, M.H. Processing methods of ultrathin poly(epsilon-caprolactone) films for tissue engineering applications. Biomacromolecules **8,** 807, 2007.
33. Serrano, M.-C., Pagani, R., Vallet-Regí, M., Peña, J., Comas, J.-V., and Portolés, M.-T. Nitric oxide production by endothelial cells derived from blood progenitors cultured on NaOH-treated polycaprolactone films: a biofunctionality study. Acta Biomater **5,** 2045, 2009.
34. Zhang, Z.Y., Teoh, S.H., Chong, M.S., Schantz, J.T., Fisk, N.M., Choolani, M.A., and Chan, J. Superior osteogenic capacity for bone tissue engineering of fetal compared with perinatal and adult mesenchymal stem cells. Stem Cells **27,** 126, 2009.
35. Tocce, E.J., Smirnov, V.K., Kibalov, D.S., Liliensiek, S.J., Murphy, C.J., and Nealey, P.F. The ability of corneal epithelial cells to recognize high aspect ratio nanostructures. Biomaterials **31,** 4064, 2010.
36. Tay, C.Y., Yu, H., Pal, M., Leong, W.S., Tan, N.S., Ng, K.W., Leong, D.T., and Tan, L.P. Micropatterned matrix directs differentiation of human mesenchymal stem cells towards myocardial lineage. Exp Cell Res **316,** 1159, 2010.
37. Kim, S.H., Ha, H.J., Ko, Y.K., Yoon, S.J., Rhee, J.M., Kim, M.S., Lee, H.B., and Khang, G. Correlation of proliferation, morphology and biological responses of fibroblasts on LDPE with different surface wettability. J Biomater Sci Polym Ed **18,** 609, 2007.
38. Greener, J., Tsou, A.H., and Blanton, T.N. Physical and microstructural effects of heat setting in polyester films. Polym Eng Sci **39,** 2403, 1999.
39. Tokiwa, Y., Calabia, B.P., Ugwu, C.U., and Aiba, S. Biodegradability of plastics. Int J Mol Sci **10,** 3722, 2009.
40. Tschoegl, N.W., Knauss, W.G., and Emri, I. Poisson's ratio in linear viscoelasticity - a critical review. Mech Time Depend Mater **6,** 3, 2002.
41. Sweeney, J., and Ward, I.M. The modeling of multiaxial necking in polypropylene using a sliplink cross-link theory. J Rheol **39,** 861, 1995.
42. Drevelle, O., Bergeron, E., Senta, H., Lauzon, M.A., Roux, S., Grenier, G., and Faucheux, N. Effect of functionalized polycaprolactone on the behaviour of murine preosteoblasts. Biomaterials **31,** 6468, 2010.
43. Wolansky, G., and Marmur, A. Apparent contact angles on rough surfaces: the Wenzel equation revisited. Colloid Surface A **156,** 381, 1999.
44. Kim, G.H. Electrospun PCL nanofibers with anisotropic mechanical properties as a biomedical scaffold. Biomed Mater **3**, 025010, 2008.
45. Zhang, Z.Y., Teoh, S.H., Hui, J.H., Fisk, N.M., Choolani, M., and Chan, J.K. The potential of human fetal mesenchymal stem cells for off-the-shelf bone tissue engineering application. Biomaterials **33,** 2656, 2012.
46. Lim, J.Y., and Donahue, H.J. Cell sensing and response to micro- and nanostructured surfaces produced by chemical and topographic patterning. Tissue Eng **13,** 1879, 2007.
47. Tsai, W.B., Ting, Y.C., Yang, J.Y., Lai, J.Y., and Liu, H.L. Fibronectin modulates the morphology of osteoblast-like cells (MG-63) on nano-grooved substrates. J Mater Sci Mater Med **20,** 1367, 2009.
48. Kim, D.H., Han, K., Gupta, K., Kwon, K.W., Suh, K.Y., and Levchenko, A. Mechanosensitivity of fibroblast cell shape and movement to anisotropic substratum topography gradients. Biomaterials **30,** 5433, 2009.
49. Yeong, W.Y., Yu, H.Y., Lim, K.P., Ng, K.L.G., Boey, Y.C.F., Subbu, V.S., and Tan, L.P. Multiscale topological guidance for cell alignment via direct laser writing on biodegradable polymer. Tissue Eng Part C Methods **16,** 1011, 2010.
50. Williams, C., Xie, A.W., Yamato, M., Okano, T., and Wong, J.Y. Stacking of aligned cell sheets for layer-by-layer control of complex tissue structure. Biomaterials **32,** 5625, 2011.
51. Gomez, N., Chen, S.C., and Schmidt, C.E. Polarization of hippocampal neurons with competitive surface stimuli: contact guidance cues are preferred over chemical ligands. J R Soc Interface **4,** 223, 2007.

Address correspondence to:
Swee Hin Teoh, PhD
Division of Bioengineering, School of Chemical and Biomedical Engineering
Nanyang Technological University
Singapore 637459
Singapore

E-mail: teohsh@ntu.edu.sg

Jerry Kok Yen Chan, PhD
Department of Reproductive Medicine
KK Women's and Children's Hospital
100 Buikit Timah Road
Singapore 229899
Singapore

E-mail: jerrychan@nus.edu.sg

Received: August 2, 2012
Accepted: November 27, 2012
Online Publication Date: January 4, 2013